PROTEINS: Structure, Function, and Bioinformatics 64:513–523 (2006)

Equilibrium Heat-induced Denaturation of Chitinase 40 from *Streptomyces thermoviolaceus*

Serapion Pyrpassopoulos,[1] Metaxia Vlassi,[1] Achilleas Tsortos,[1] Yannis Papanikolau,[2] Kyriacos Petratos,[2] Constantinos E. Vorgias,[3] and George Nounesis[1]*

[1]*National Centre for Scientific Research "Demokritos,"153 10 Aghia Paraskevi, Greece*
[2]*Institute of Molecular Biology and Biotechnology, Foundation for Research and Technology, 711 10 Heraklion, Greece*
[3]*Department of Biology, National and Kapodistrian University of Athens, 157 84 Panepistimiopolis-Zografou, Greece*

ABSTRACT **High-precision differential scanning calorimetry (DSC) and circular dichroism (CD) have been employed to study the thermal unfolding of chitinase 40 (Chi40) from *Streptomyces thermoviolaceus*. Chi40 belongs to family 18 of glycosyl hydrolase superfamily bearing a catalytic domain with a "TIM barrel"-like fold, which exhibits deviations from the $(\beta/\alpha)_8$ fold. The thermal unfolding is reversible at pH = 8.0 and 9.0. The denatured state is characterized by extensive structural changes with respect to the native. The process is characterized by slow relaxation kinetics. Even slower refolding rates are recorded upon cooling. It is shown that the denaturation calorimetric data obtained at slow heating rate (0.17 K/min) are in excellent agreement with equilibrium data obtained by extrapolation of the experimental results to zero scanning rate. Analysis of the DSC results reveals that the experimental data can be successfully fitted using either a nontwo-state sequential model involving one equilibrium intermediate, or an independent transitions model involving the unfolding of two Chi40 energetic domains to intermediate states. The stability of the native state with respect to the final denatured state is estimated, ΔG = 24.0 kcal/mol at 25°C. The thermal results are in agreement with previous findings from chemical denaturation studies of a wide variety of $(\beta/\alpha)_8$ barrel proteins, that their unfolding is a nontwo-state process, always involving at least one unfolding intermediate. Proteins 2006;64:513–523.**

Key words: thermal unfolding; TIM-barrel protein; unfolding intermediate state; calorimetry; circular dichroism

INTRODUCTION

Chitinases (EC 3.2.1.14) are chitinolytic enzymes that have been detected in a wide range of organisms such as fungi, crustaceans, and insects. The natural polymer chitin is abundant in nature as it is an important element in the structure of fungal cell walls and arthropod exoskeletons. It is the linear insoluble β-1,4-linked polymer of N-acetyl-β-D-glucosamine. Chitinases cleave the β-1,4-glycosidic bonds to generate eventually di-N-acetyl-chitobiose. Organisms that do not contain chitin such as archaea, bacteria, viruses, higher plants, animals, and humans have also been found to express chitinases. According to the mode of chitin hydrolysis, chitinases have been classified as random, endo-, and exo- chitinases, while on the basis of primary structure comparisons, they have been classified in families 18 and 19 of the glycosyl hydrolase superfamily. Chitobiases, which are also chitin hydrolases, have been classified in family 20. Several common properties are shared by the members of a family such as the folding of the catalytic domain, the substrate specificity, and the stereochemistry of the reaction, as well as the catalytic mechanism.[1,2]

The structure and the mechanism of chitin degradation has been well studied for the enzymes chitinase A and B and chitobiase from the mesophilic soil bacterium *Serratia marcescens*.[3–8] The structure of chitinase A (pdb code 1EDQ[9]) comprises a catalytic TIM-barrel domain, which exhibits several deviations (mainly insertions) from the $(\beta/\alpha)_8$ fold. The most notable of these deviations is the inclusion of the so-called "α + β" structural domain (pdb code 1CTN, residues 444–516[3]), which, nevertheless, seems to be functionally integrated to the catalytic domain of chitinase A. Amino acid residues of the α + β domain participate in critical binding of the substrate $(NAG)_8$ by the enzyme.[8] So far, no structural or other biophysical data have been accumulated for chitinases from thermophilic organisms. Christodoulou et al.[10] have recently shown a new procedure for the large-scale purification of the recombinant thermostable chitinase (Chi40) from *S. thermoviolaceus* expressed in *Escherichia coli*. The chitinolytic system of the thermostable bacterium *Streptomyces thermoviolaceus* OPC-520 consists of four chitinase genes (*chi40*, *chi35*, *chi30*, and *chi25*) and two N-acetyl-β-glucosaminidase genes (*nagA* and *nagB*). Chi40 belongs to family 18. Although the structure of the protein is not yet known, based upon the structures of other chitinases of the same family such as: chitinase A (1EDQ at 1.55 Å resolution),[9] chitinase B (1E6Z),[11] chitinase A1 (1LL4),[12] and chitotriosidase (1LG1),[13] it can be expected that the catalytic domain of Chi40 is most likely a type $(\beta/\alpha)_8$ barrel.

*Correspondence to: George Nounesis, National Centre for Scientific Research "Demokritos," 153 10 Aghia Paraskevi, Greece. E-mail: nounesis@rrp.demokritos.gr

Received 23 June 2005; Revised 23 January 2006; Accepted 15 February 2006

Published online 5 May 2006 in Wiley InterScience (www.interscience.wiley.com). DOI: 10.1002/prot.21003

Structural as well as stability studies of $(\beta/\alpha)_8$ barrel proteins present substantial scientific interest for two main reasons. First, they catalyze a wide range of reactions and are thus attractive for biotechnological research. Second, there exists a multitude of proteins with low homology between them (over 10% of the enzymes with known structures) that they all exhibit common β/α barrel structures.[14] The folding of eight-stranded $(\beta/\alpha)_8$ or TIM barrels has thus attracted considerable experimental and theoretical attention, and important research results have sprung out from research efforts in this direction.[15] Chemical unfolding/refolding studies along with numerical simulations and modeling have in several cases demonstrated slow relaxation kinetics as well as the existence of at least one equilibrium intermediate unfolding state (a series of intermediates for the refolding pathway). Two intermediates have been identified in the case of the α subunit of tryptophan synthase (αTS). The first retains most of the native's secondary structure, while the second is structurally very close to the unfolded state.[16–18] Simulation studies have indicated that a loose six-stranded βα-barrel may well be a possible N-terminal folding intermediate,[19] providing thus evidence for a 6 + 2 folding mechanism. Recent hydrogen exchange mass spectrometry studies have shown that the (β/α)(1-3)β(4) module appears to represent the minimum subcore of stability of the second (the unstructured) intermediate pointing towards a possible 4 + 2 + 2 folding mechanism.[20] Fragment complementation analysis of N-(5′-Phosphoribosyl)anthranilate Isomerase (PRAI) from *Saccharomyces cerevisiae* point towards the existence of an unfolding intermediate as well.[21] Guanidinium chloride-induced denaturation of PRAI from *Escherichia coli* has revealed slow relaxation kinetics, and even though circular dichroism spectroscopy could only detect a two-state cooperative unfolding transition, kinetic studies demonstrated the existence of at least one equilibrium intermediate. A nonsequential unfolding model has been proposed to describe these results.[22] Analogous is the case of rabbit muscle triosephosphate isomerase where an intermediate characterized by low stability has also been shown to exist only after using kinetic techniques.[23] So far, no thermal denaturation studies of chitinases have been reported. This may be due to the fact that extended hydrophobic areas become exposed to the solvent upon denaturation leading to aggregation and irreversibility of the thermal transition. In the present study, calorimetric and CD experiments of the thermally induced reversible unfolding of Chi40 from *Streptomyces thermoviolaceus* provide evidence for a non-two-state denaturation process characterized by slow relaxation kinetics. To our knowledge, this is the first report for the reversible heat denaturation of a chitinase containing a TIM-like catalytic domain.

MATERIALS AND METHODS

Materials

The column chromatography media were purchased from Pharmacia, and all the other chemicals were from Sigma or Merck, in the highest analytical grade.

Cloning of Chi40 in *E. coli*

The gene for a thermostable Chi40 from *Streptomyces thermoviolaceus* was cloned as described in ref. 10.

Overproduction and Purification of Chi40 Protein Secreted in the Culture Medium

The plasmid pECHChi40-9 was introduced in BL21*trx*B(DE3) cells that were grown in LB medium in the presence of ampicillin and kanamycin (kan), each at 50 μg/mL. The cell culture was grown under strong agitation at 37°C, overnight. The following day the bacteria were collected by centrifugation and kept frozen thereafter, while the supernatant medium was immediately adjusted to 0.5 M ammonium sulphate in buffer A (20 mM Tris-HCl pH 8.0, 1 mM EDTA, 0.1 mM PMSF). The solution was loaded on a 20-mL Phenyl-Sepharose column previously equilibrated in buffer B (20 mM Tris-HCl pH 8.0, 0.5 M ammonium sulphate). After having completed the loading of the sample, the column was washed with five volumes buffer B. Bound proteins were eluted with a 200-mL 0.5–0 M ammonium sulphate descending gradient in buffer A and finally with 50 mL buffer A. Chi40 containing fractions were detected by activity assays using pNp-$(NAG)_2$ and verified by 0.1% SDS-12.5% PAGE analysis. The Chi40 fractions were pooled and applied on a 10-mL Q-High Performance column, equilibrated in buffer B. Bound Chi40 was eluted with a 200 mL 0–0.5 M NaCl gradient in buffer B, and fractions containing highly pure Chi40 protein were combined and kept at 4°C, for at least 1 year.

Chi40 Activity Assays Using p-Nitrophenyl-β-D-N,N′-Diacetylchitobiose (pNp-NAG_2)

Activity assays were carried out in a reaction volume of 1 mL in a glass cuvette equilibrated to the appropriate temperature. Activity was monitored by the release of the *p*-nitrophenyl group from the substrate resulting in a yellow color detected spectrophotometrically at 405 nm. The activity units (1 μmol/min) were calculated using the molar extinction coefficient for the *p*-nitrophenyl group ($E_{405\text{nm}} = 18.5\ \text{mM}^{-1}\,\text{cm}^{-1}$).

Differential Scanning Calorimetry (DSC)

For the high-sensitivity calorimetric measurements the VP DSC calorimeter was employed (Microcal, Northampton, MA).[24] Protein concentrations used in the DSC studies varied between 0.3 and 2.0 mg/mL. Protein samples and buffer reference solutions were properly degassed and carefully loaded into the cells to avoid bubble formation. Four to five reference scans with buffer filled cells (sample and reference cell volume is 0.523 mL) preceded each sample run to achieve near perfect baseline repeatability. A typical DSC experiment consisted of a heating scan at a programmed heating rate followed by a second heating scan, which probed the reversibility of the transitions under study. Whenever needed, the difference in the heat capacity between the initial and final states was modeled by a sigmoidal chemical baseline.[25] The calorimetric data were corrected for the instruments response time[26] and

analyzed via nonlinear least squares fitting procedures of the ORIGIN® 5.0 software.

Circular Dichroism Spectroscopy (CD)

CD measurements were conducted using a JASCO-715 spectropolarimeter with a Peltier-type cell holder, which allows for temperature control. Wavelength scans in the far (190 to 260 nm) and the near (260 to 360 nm) UV regions were performed in Quartz SUPRASIL (HELLMA) precision cells of 0.1- and 1-cm path length, respectively. Each spectrum was obtained by averaging five to eight successive accumulations with a wavelength step of 0.2 nm at a rate of 20 nm min^{-1}, response time 1 s, and band width 1 nm. Buffer spectra were accumulated and subtracted from the sample scans. The absorption spectra were recorded selecting the UV (single) mode of the instrument. CD experiments involving thermal scanning have been carried out in the range from 20 to 90°C, at 213.5, 222, and 225 nm, and heating scan rates ranging from 0.3 to 2.5 K/min.

Sequence Alignments

Sequence alignments were performed using the program ClustalW[27] via the ClustalW Web service at the European Bioinformatics Institute (http://www.ebi.ac.uk/clustalw). The ESPript utility[28] was used for constructing Figure 12. The sequence alignment produced by ClustalW and the PDB entry: 1CTN[3] corresponding to the crystal structure of chitinase A was provided as the input.

RESULTS

DSC

The heat denaturation of Chi40 was studied by high-sensitivity DSC. Reversible thermal unfolding was found at pH = 8.0 and 9.0. After consecutive heating DSC scans at heating scan rates u = 1.5 K/min, near-perfect reversibility (99%) of the thermal transition, was recorded at pH 9.0 (10 mM Tris-HCl) [Fig. 1(A)]. At pH 9.0 (50 mM Na-Borate) the reversibility was ~90% [Fig. 1(B)]. At pH 8.0 (20 mM Na-Phosphate) the reversibility of the calorimetric data was ~87%. At various other pH values the DSC curves revealed irreversible thermal processes described by heat capacity peaks whose shapes were visibly affected by on-going aggregation in the denatured state. Profiles of the excess heat capacity ($\langle \Delta C_p \rangle$) versus temperature ($T$) have been obtained at pH 9.0 for various values of the total protein concentration (C_t) and DSC scan rates. No dependence was found between the values of C_t and the experimentally obtained values of T_m (temperature for maximum $\langle \Delta C_p \rangle$ value), indicative that the peaks describe the unfolding of a monomeric protein. On the other hand, a pronounced dependence of T_m upon u was observed, which in turn, is an indication that equilibrium relaxation during the denaturation process is slow. The reversibility of the thermal transition was tested against various DSC heating rates. The population of the molecules at 10 mM Tris-HCl buffer refolding to the native state upon cooling varied between 90 (for the smallest values of u) and 99%, of the total population. This high degree of reversibility

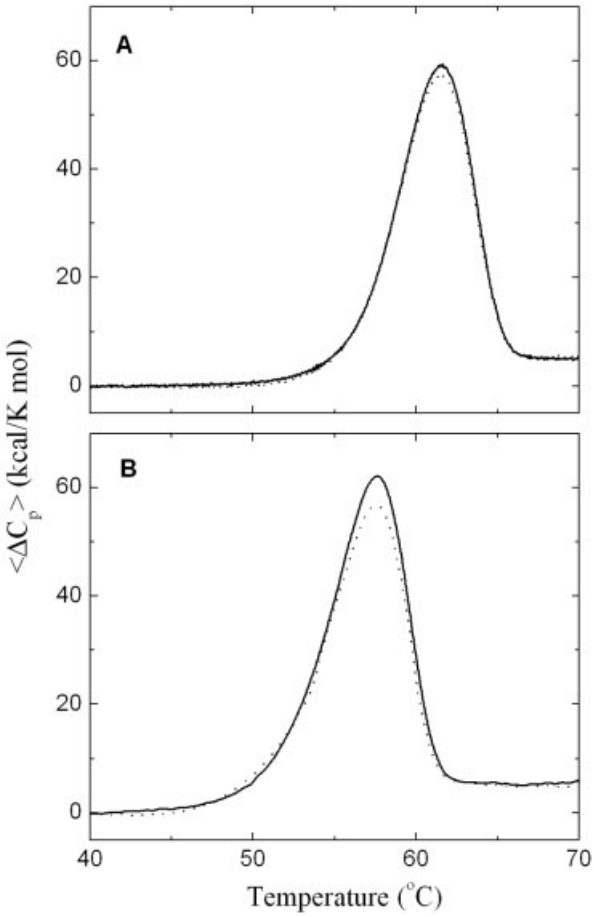

Fig. 1. DSC profiles for consecutive heating scans of Chi40 at pH 9.0 and u = 1.5 K/min (**A**) 10 mM Tris-HCl and (**B**) 50 mM Na-borate. The solid lines represent the first heating scan and the dotted lines the second.

demonstrates that irreversible unfolding is probably directly related to the amount of time the protein sample is kept at high temperatures in the denatured state. Irreversible processes are thus slow (most likely due to aggregation phenomena) and do not contribute to the apparent kinetics of the denaturation. The calorimetric curves for five different DSC heating rates (u = 0.17, 0.33, 0.5, 1.0, and 1.5 K/min) are presented in Figure 2, while the corresponding parameters, corrected for the instrument's response time,[26] are listed in Table I. As can be readily seen in Table I, the experimental calorimetric results obtained at pH 9.0 for the two different buffers (10 mM Tris-HCl and 50 mM Na-borate) are in very good agreement. Specifically, the values of the total enthalpy change (ΔH_{cal}) and the heat capacity change (ΔC_p) coincide within the experimental error. This is indicative that in the case of samples in dilute Tris-HCl, buffer ionization effects have minimal contribution to the calorimetric values of ΔH_{cal}. Due to the consistency of the calorimetric results for the various buffer conditions we present the analysis of only the experimental data obtained for the Chi40 samples at 10 mM Tris-HCl buffer, which exhibited optimal reversibility of the thermal unfolding process.

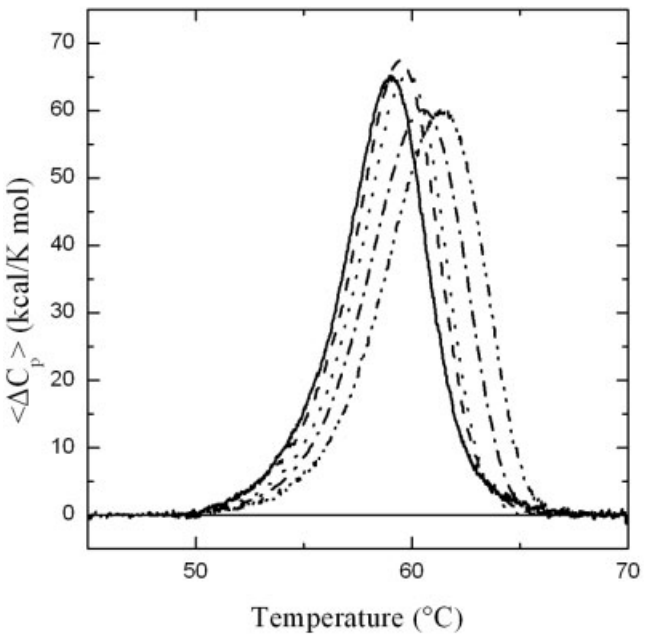

Fig. 2. DSC profiles for the thermally induced reversible denaturation of Chi40 at pH 9.0, 10 mM Tris-HCl at five different heating scan rates *u*: 0.17 K/min (solid line), 0.33 K/min (dashed line), 0.5 K/min (dotted line), 1.0 K/min (dot-dashed line) and 1.5 K/min (dot-dot-dashed line).

Because the kinetic dependence of the calorimetric parameters can be exclusively attributed to slow relaxation for attaining thermodynamic equilibrium during the denaturation process, we have attempted to extrapolate the experimental results at zero DSC heating rate. It has been shown that:[26,29,30]

$$\langle \Delta C_p(T)\rangle_{\mathrm{eq}} = \langle \Delta C_p(u,T)\rangle_{\mathrm{exp}} + u \cdot \tau_C(T) \cdot \frac{d\langle \Delta C_p(u,T)\rangle_{\mathrm{exp}}}{dT} \quad (1)$$

$$\langle \Delta H(T)\rangle_{\mathrm{eq}} = \langle \Delta H(u,T)\rangle_{\mathrm{exp}} + u \cdot \tau_{\mathrm{H}}(T) \cdot \langle \Delta C_p(u,T)\rangle_{\mathrm{exp}} \quad (2)$$

Here, $\langle \Delta C_p(T)\rangle_{\mathrm{eq}}$ and $\langle \Delta H(T)\rangle_{\mathrm{eq}}$ are the equilibrium values of the heat capacity and the enthalpy change, respectively, at temperature T, while $\langle \Delta C_p(T)\rangle_{\mathrm{exp}}$ and $\langle \Delta H(T)\rangle_{\mathrm{exp}}$ are the corresponding experimental results. $\tau_C(T)$ and $\tau_H(T)$ are the corresponding relaxation times for C_p and ΔH. It must be noted that Equations (1) and (2) are only valid for linear responses, that is, for small deviations from equilibrium.[26,31] Linear fitting attempts of the $\langle \Delta H(T)\rangle_{\mathrm{exp}}$ versus $[u \cdot \langle \Delta C_p(T)\rangle_{\mathrm{exp}}]$ data in the temperature range from 5% to 95% completeness of the denaturation process, for the five different experimental values of u, yield successful fits characterized by correlation coefficients ranging between 0.96 and 0.99 (Fig. 3). The fitting procedure leads to estimates of $\langle \Delta H(T)\rangle_{\mathrm{eq}}$ and $\tau_H(T)$, and thus by direct differentiation with respect to T, the curve of $\langle \Delta C_p(T)\rangle_{\mathrm{eq}}$ can be obtained. This result is illustrated in Figure 4, along with the curve of $\langle \Delta C_p(T)\rangle_{\mathrm{eq}}$, which can be directly estimated from Equation (1) in a similar fashion. The experimental DSC profile at $u = 0.17$ K/min is also shown to facilitate direct comparisons. It can be deduced that, within the experimental error, the DSC curve for the slowest heating rate coincides nicely with the equilibrium peak obtained from the extrapolation of the experimental results to $u = 0$. More specifically, the value of $T_m = 59.0 \pm 0.5$°C is obtained from the curve of $\langle \Delta C_p(T)\rangle_{\mathrm{eq}}$ [Eq. (1)]. Accordingly, from $[d(\langle \Delta H(T)\rangle_{\mathrm{eq}}]/dT$ [Eq. (2)] the value of $T_m = 58.5 \pm 0.5$°C is estimated. Finally, from the experimental results for $u = 0.17$ K/min the value $T_m = 59.0 \pm 0.5$°C is measured. All these results are in good accord.

From the calorimetric parameters presented in Table I, it can be observed that the value of the ratio $\Delta H_{\mathrm{cal}}/\Delta H_{\mathrm{vH}}$ approaches the value of 2 as u approaches the slowest rates. Here, ΔH_{cal} is the experimental calorimetric enthalpy change and ΔH_{vH} is the van't Hoff enthalpy change.[32] This result provides strong evidence that the thermal unfolding of Chi40 is not a two-state process.[33–35] For accuracy, we have used the double deconvolution method for the analysis of our data,[35] which provided evidence that the thermal denaturation process has one intermediate state. We have thus attempted to analyze our results by employing a model for the thermal unfolding involving one intermediate state between the native and the denatured states.

$$N \rightleftarrows I \rightleftarrows U \quad (3)$$

Here, N is the native, I is the intermediate, and U is the final denatured state. To deconvolute the calorimetric $\langle \Delta C_p\rangle$ peak to its constituents, we have employed the following equation[36–38] to fit the data at $u = 0.17$ K/min:

$$\langle \Delta C_p\rangle = \sum_i (\Delta_0^i C_p P_i) + \frac{1}{RT^2}\sum_i (\Delta_0^i H^2 F_i) - \frac{1}{RT^2}\left(\sum_i \Delta_0^i H F_i\right)^2 \quad (4)$$

Here, the index i may take the values {0, 1, 2}, corresponding to the states N, I, and U, respectively. $\Delta_i^0 H$ and $\Delta_i^0 C_p$ represent the change in enthalpy and heat capacity, respectively, of state i with respect to the native state, while F_i represents the population of each thermodynamic state i.

$$F_i = K_i \Big/ \left(1 + \sum_{j=1}^{n} K_j\right) \quad (5)$$

$$K_i = \exp\left(-\frac{\Delta_0^i H}{RT}\left(1 - \frac{T}{T_i}\right) - \frac{\Delta_0^i C_p}{RT}\left(T - T_i - T\ln\frac{T}{T_i}\right)\right) \quad (6)$$

T_i is the characteristic temperature for state i for which K_i is 1. The fitting attempts of the experimental DSC profile for $u = 0.17$ K/min as well as of the $\langle \Delta C_p(T)\rangle_{\mathrm{eq}}$ curve (obtained at $u = 0$) with Equation (4) was successful (Fig. 5). The values for all the fitted parameters are presented in Table II. The agreement between the fitted parameters for the experimental data set and those for the simulated curve at $u = 0$ is excellent, reaffirming that the $u = 0.17$ K/min DSC profile is close to the equilibrium behavior. Based on the results presented in Table II, the population

TABLE I. DSC Results

u (K/min)	ΔH_{cal} (kcal/mol)	$T_{1/2}$ (°C)	$\langle \Delta C_p(T_{1/2}) \rangle$ (kcal/K mol)	ΔC_p (kcal/K mol)	ΔH_{vH} (kcal/mol)	$\Delta H_{cal}/\Delta H_{vH}$
0.17[a]	333.0 ± 16.7	58.7 ± 0.5	63.74	5.6 ± 0.1	167.6	1.99
0.33[a]	348.3 ± 16.9	59.1 ± 0.5	65.92	5.5 ± 0.1	166.0	2.10
0.5[a]	332.7 ± 18.3	59.3 ± 0.5	63.45	5.6 ± 0.1	167.6	1.99
1.0[a]	342.9 ± 18.6	60.0 ± 0.5	58.69	5.7 ± 0.1	151.0	2.27
1.5[a]	350.6 ± 22.7	60.8 ± 0.6	58.42	5.6 ± 0.1	147.7	2.37
1.5[b]	355.7 ± 23.6	56.7 ± 0.5	58.90	5.4 ± 0.1	143.2	2.48
1.5[c]	349.8 ± 24.5	59.9 ± 0.6	64.32	5.5 ± 0.1	162.1	2.16

Experimental calorimetric results for the thermal unfolding of Chi40 at various buffers and heating scan rates. ΔH_{vH}, is the van't Hoff enthalpy change.[32] The ratio $\Delta H_{cal}/\Delta H_{vH}$ is also listed.
[a]pH 9.0, 10 mM Tris-HCl.
[b]pH 9.0, 50 mM Na-borate.
[c]pH 8.0, 20 mM Na-phosphate.

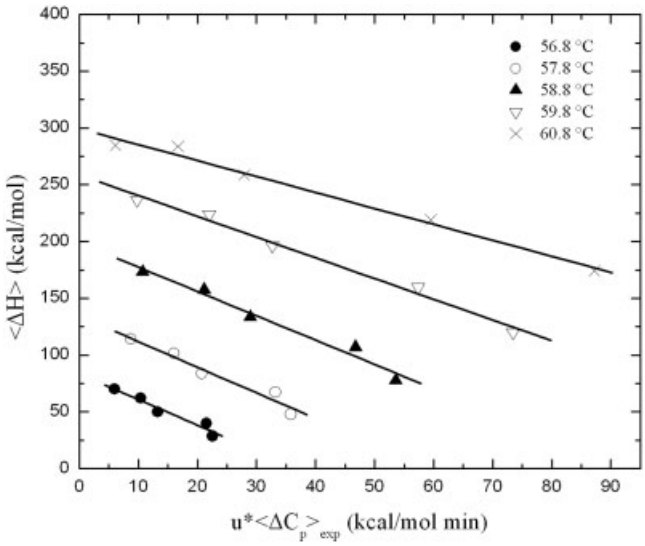

Fig. 3. Linear fits of the experimental data $\langle \Delta H(T) \rangle_{exp}$ versus u. $\langle \Delta C_p(T) \rangle_{exp}$ based on Equation (2), for five different values of the temperature: 56.8, 57.8, 58.8, 59.8, and 60.8°C.

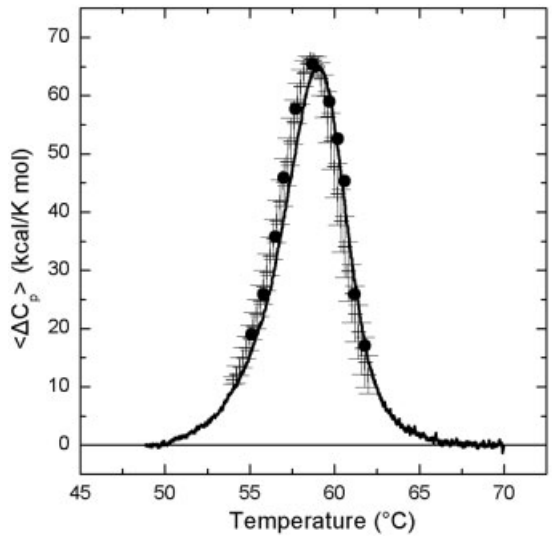

Fig. 4. The experimental DSC peak for u = 0.17 K/min (solid line). Also displayed is the profile $\langle \Delta C_p(T) \rangle_{eq}$ as derived by differentiation of Equation (2) [(+) symbol with the corresponding error bars] and also as derived directly from Equation (1) (●). In the latter case, only a few representative points are drawn for reasons of clarity.

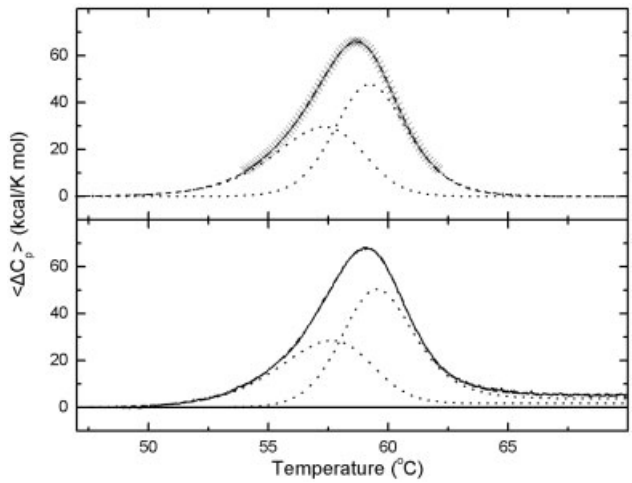

Fig. 5. Nonlinear least squares fit of the $\langle \Delta C_p \rangle$ versus T profiles with Equation (4), involving two consecutive thermal transitions $N \rightarrow I$ and $I \rightarrow D$. Upper panel: the data $\langle \Delta C_p(T) \rangle_{eq}$ versus T obtained by extrapolating the experimental results to $u \rightarrow 0$ [(+) symbol] are fitted by Equation (4) (dashed line represents the best fit). The two consecutive thermal transitions are depicted by the dotted lines. Lower panel: the experimental data $\langle \Delta C_p(T) \rangle_{exp}$ obtained at u = 0.17 K/min (solid line) are fitted by Equation (4) (dashed line). The dotted lines represent once again the individual consecutive thermal transitions.

of protein molecules at each state can be estimated as a function of T. These results are illustrated in Figure 6(A).

The calorimetric data have also been analyzed using an independent transitions model, assuming that two energetically independent domains of Chi40 unfold into two distinct partially unfolded intermediates.[39,40]

$$\begin{array}{ccccc} & & A_UB_N & & \\ & \nearrow & & \searrow & \\ A_NB_N & & & & A_UB_U \\ & \searrow & & \nearrow & \\ & & A_NB_U & & \end{array} \qquad (7)$$

Here, A and B are the two energetically independent domains of Chi40, the subscript N stands for native and U for unfolded states. The fits were as successful as for the sequential model. The fitting parameters are listed in Table II. It is thus becoming apparent that the DSC data alone cannot provide a distinction between the two mod-

TABLE II. Results from the Fitting of the DSC Profiles

	u (K/min)	i	T_i (°C)	$\Delta_0^i H$ (kcal/mol)	$\Delta_0^i S$ (kcal/K mol)	$\Delta_0^i C_p$ (kcal/K mol)
Sequential model	0	1	57.1	147.1	0.5	
	(extrapolation)	2	58.2	337.6	1.0	
	0.17	1	57.3	141.5	0.4	1.8
	(experimental)	2	58.5	334.3	1.0	5.5
Independent transitions model	0	A	57.0	131.0	0.4	
	(extrapolation)	B	58.9	211.9	0.6	
	0.17	A	57.2	125.0	0.4	2.0
	(experimental)	B	59.1	212.0	0.6	3.5

Thermodynamic parameters for the thermal unfolding of Chi40 resulting from fitting the experimental data for u = 0.17 K/min as well as the set of data obtained by extrapolation to u = 0 with the model predicting one intermediate unfolding state [Eq. (4)]. As pointed out in the text, $i = 1$ denotes unfolding transition to the intermediate state and $i = 2$, the transition from the native to the denatured state (sequential model), A and B correspond to the two energetically independent domains (independent transitions model).

els.[40] The population of protein molecules at the various states of the independent-transitions model are illustrated as a function of temperature in Figure 6(B).

The per-residue values of the thermodynamic parameters are ΔC_p = 14.8 cal/K mol residue and ΔH = 0.89 kcal/mol residue. These values agree well with what has been reported in the literature (ΔC_p = 14.7 ± 2.2 cal/K mol residue and ΔH = 0.77 ± 0.09 kcal/mol residue) for extended thermal unfolding of protein molecules comparable in size to Chi40.[39,41,42] We have estimated the values for ΔH and ΔS at 110°C, the temperature at which the corresponding parameters for extended thermal unfolding of spherines are expected to converge, considering a constant and thus temperature-independent ΔC_p.[43] For Chi40, we find ΔH (110°C) = 6.6 ± 0.3 kJ/mol residue and ΔS (110°C) = 19.3 ± 0.8 kJ/K mol residue, which compare well with what was predicted by Privalov:[43] ΔH (110°C) = 6.3 ± 0.2 kJ/mol residue and ΔS (110°C) = 17.6 ± 0.6 kJ/K mol residue.

Based on the experimental results for u = 0.17 K/min presented in Table I, the stability curve for Chi40 can be constructed (Fig. 7).[44] The stability of the native state N with respect to the final denatured state U calculated at 25°C is ΔG = 24.0 ± 2.9 kcal/mol. Depending on the thermodynamic model employed, based on the fitting results presented in Table II, the stability at 25°C for the unfolding transition to the intermediate states can be obtained: ΔG^1 = 13.3 kcal/mol in the case of the sequential model, and ΔG^A = 9.0 kcal/mol and ΔG^B = 15.0 kcal/mol in the case of the two-independent transitions model.

CD Spectroscopy

CD spectroscopy has been employed to investigate structural changes during the thermal unfolding of Chi40. Figure 8 displays the far-UV CD spectra in the native (at T = 25°C) and the denatured (at T = 70°C) states. It is evident that the spectrum for the denatured molecule carries a lot of resemblance to the corresponding far-UV spectra obtained for other proteins undergoing extended thermal denaturation.[42] They are characterized by a largely broadened and attenuated negative peak around 220 nm and a sharply intense minimum in the neighborhood of 200 nm (characteristic of random coil spectra). The average values obtained using SELCON,[45] CONTIN,[46] K2D,[47] and CDNN[48,49] algorithms for estimating the percentage of the secondary structure elements in the native and the denatured state, reveal a loss in α-helical structure of more than 15%.

Near-UV CD spectra before and after the thermal unfolding are presented in Figure 9. These spectra demonstrate the almost complete loss of tertiary structure for Chi40. Far- and near-UV measurements have been carried out for several temperatures within the range of the thermal transition. It is of particular interest to note that the far-UV CD spectra exhibit an isodichroic point at λ = 213.6 nm (Fig. 10). Usually, the occurrence of an isodichroic point provides evidence, but not necessarily proof, that the thermal transition under investigation is a two-state process. In the case of Chi40, as demonstrated by the DSC results, this is clearly not the case, because the existence of an intermediate unfolding state was shown. It is thus through calorimetry and/or a combination of spectroscopic techniques that the presence of intermediate folding states can be accurately determined.

The thermal unfolding and refolding of Chi40 was also recorded in CD experiments by measuring the elipticity at constant wavelength while scanning the temperature, for consecutive heating and cooling runs at various heating/cooling rates. Characteristic results at two different heating and cooling rates u = 1.5 K/min and u = 0.17 K/min are displayed in Figure 11. It can be straightforwardly observed that the experimental curves and particularly the observed unfolding/refolding hystereses are strongly dependent upon the scanning rates. For u = 1.5 K/min the unfolding is fully reversible, while for u = 0.17 the reversibility is estimated to ~90%, which is in agreement with the DSC results. The small percentage of irreversibility may be directly associated to the time that the sample is kept at high temperatures in the denatured state.

DISCUSSION

Most often, the experimental DSC profiles, exhibit strong dependence upon the temperature scanning rates, when the thermal unfolding is irreversible.[50,51] In the case of Chi40, it is shown that a reversible DSC transition may also exhibit a dependence upon the heating rate implying

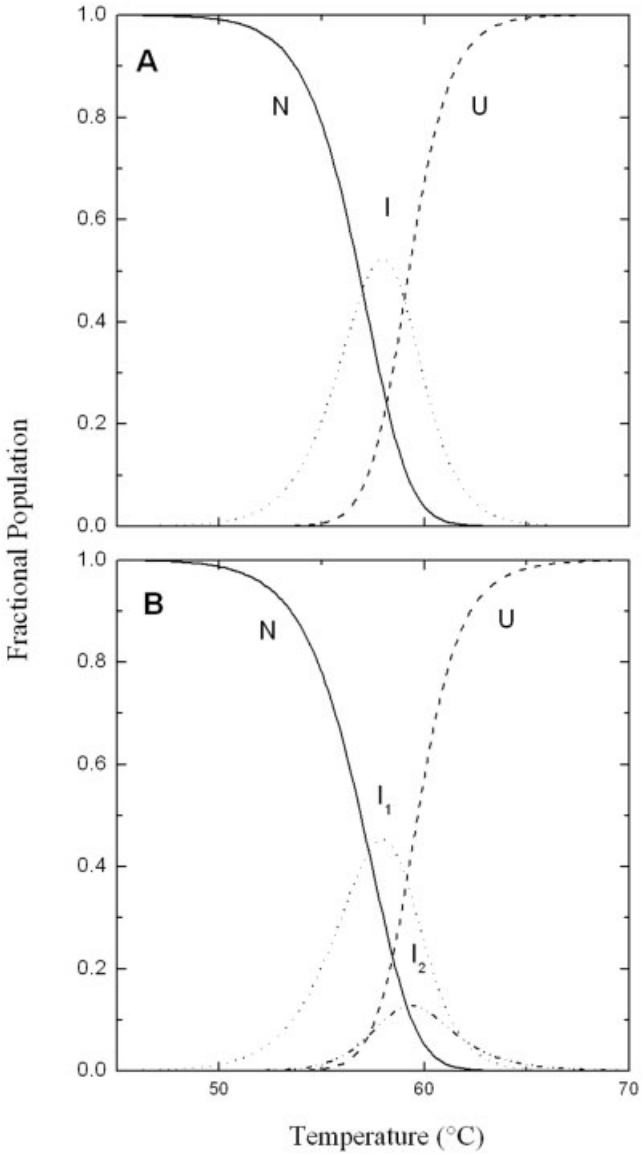

Fig. 6. (**A**) Temperature profiles of the fractional populations of protein molecules in the various states: native state *N* (solid line), unfolded state *U* (dashed line), and intermediate unfolding state *I* (dotted line). The profiles are obtained by Equation (5) using the results presented in Table II from the fitting of the experimental DSC data. (**B**) Temperature profiles of the fractional populations obtained from the fitting results of the two-independent transitions model: *N* (solid line), *U* (dashed line), first intermediate unfolding state I_1 (dotted line), and second intermediate unfolding state I_2 (dash-dotted line). The intermediate states correspond to the $A_N B_U$ and $A_U B_N$ states included in the model [Eq. (7)].

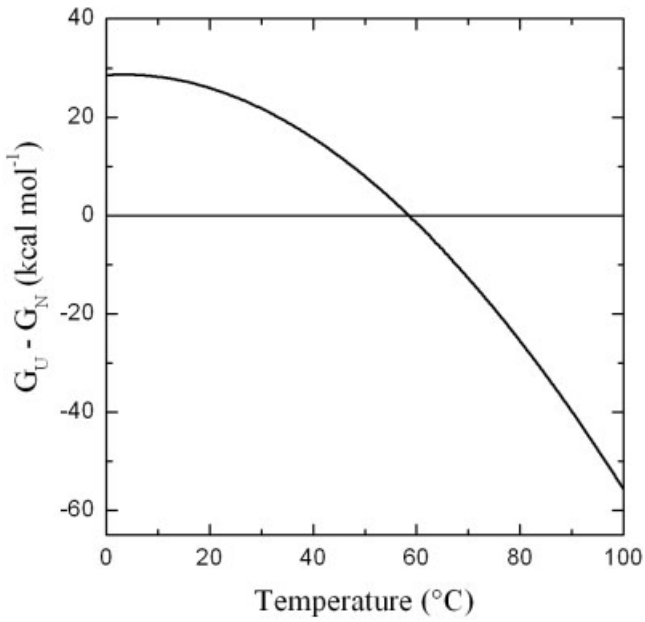

Fig. 7. Temperature profile of the free energy change $\Delta G(T)$ from the native *N* to the final denatured state *U*.

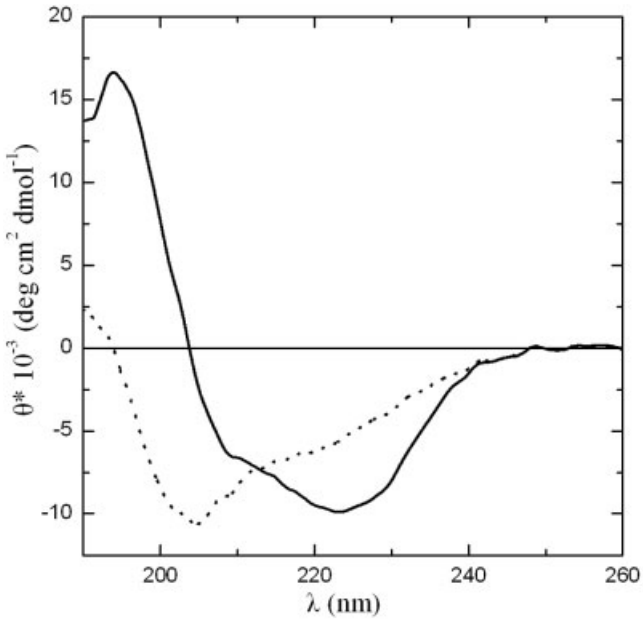

Fig. 8. Normalized far-UV CD spectra for native Chi40 at pH 9.0, 10 mM Tris-HCl at 25°C (solid line) and for thermally denatured state at 70°C (dashed line).

slow relaxation kinetics. Analogous behavior has also been observed for other proteins.[52–54] It is thus imperative that the scanning rate dependence of the experimental ($\langle \Delta C_p \rangle$ vs. T) DSC profiles must always be checked even in the case of full reversibility of the thermal unfolding. It is possible that the molecule's equilibrium relaxation rate may always be comparable to the experimental heating scan rate u.

Slow relaxation to equilibrium is usually attributed to the structural heterogeneity of the unfolding state, mainly due to the *cis–trans* isomerization of proline residues.[55] The *cis–trans* isomerization reaction of prolines is a slow process characterized by time constants between 10 and 100 s at 25°C and a high activation energy E_a ~20 kcal/mol.[55] Approximately 7% of all the proline residues in the native state of proteins of known structure are in the cis conformation.[56] It may thus be expected that the unfolding rate of large polypeptide chains may be exponentially reduced as a function of the proline residues in the

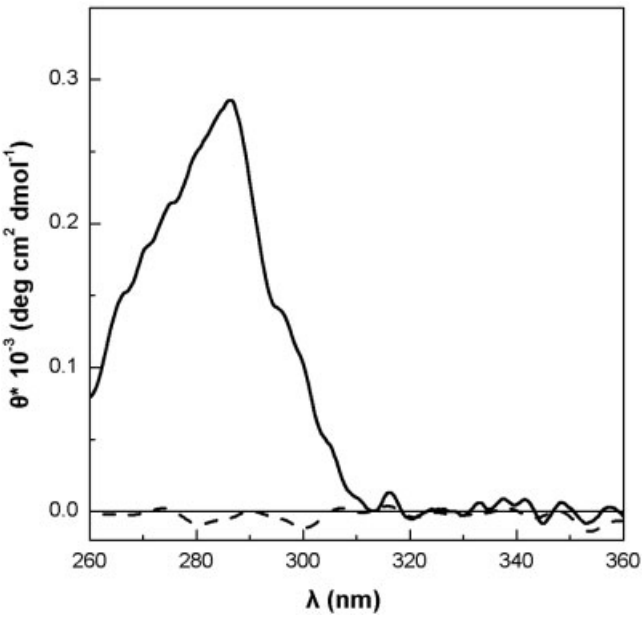

Fig. 9. Near-UV CD spectra for native Chi40 at pH 9.0, 10 mM Tris-HCl at 25°C (solid line) and for the thermally denatured state at 70°C (dashed line) depicting the complete loss of tertiary structure upon thermal unfolding.

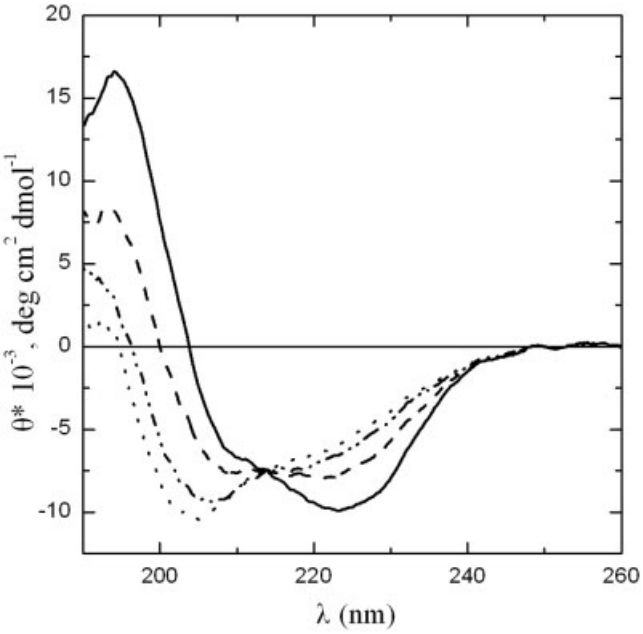

Fig. 10. Normalized far-UV CD spectra at various temperatures within the temperature range of the thermal unfolding of Chi40: 25°C (solid line); 57°C (dashed line); 60°C (dot-dot-dashed line), and 65°C (dotted line). The spectra exhibit an isodichroic point at λ = 213.6 nm. As pointed out in the text the existence of the isodichroic point is no evidence for a two-state thermal transition.

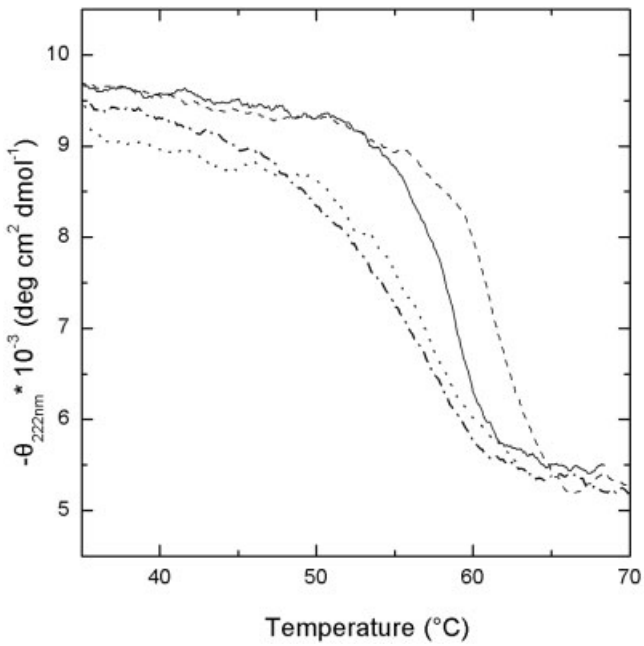

Fig. 11. Normalized temperature profiles of the elipticity at λ = 222 nm depicting the different kinetics between the thermal unfolding and the refolding (upon cooling) processes of Chi40, as well as between the various scanning rates. The solid line represents a heating scan at u = 0.17 K/min and the dashed line heating at u = 1.5 K/min. The dot-dashed profile corresponds to a cooling scan at u = 0.17 K/min and the dotted line to a cooling scan at u = 1.5 K/min.

protein sequence,[57] or, in turn, that the large number of proline residues will seriously slow down the refolding rate of a protein molecule.[58] The molecule of Chi40 contains 17 prolines, which correspond to 4.4% of the total number of amino acid residues. In fact, a *cis*-prolyl bond isomerization has been shown to dominate the folding of aTP, which is also a TIM barrel protein.[59] In addition to prolines, it has also been shown that other amino acid residues assume *cis* conformation. The *trans–cis* isomerization reaction of these residues may also be characterized by slow refolding rates.[60] Several proteins of known structures have amino acid sequences highly homologous to that of Chi40: Chitinase A from *S. marcescens* (1CTN),[3] Chitinase B *S. marcescens* (1E6Z), Chitinase A1 (1ITX),[61] Chitinase 1 (1LL4), and Chitotriosidase (1LG1). All these molecules contain a high percentage of proline and other residues in the *cis* conformation. Slow unfolding/refolding rates in large protein molecules may also be due (in addition to the *cis–trans* isomerization of the peptide bond) to the relative conformation of different structural regions during the unfolding process.[58]

The amino acid sequence of Chi40 shares high similarity with other members of family 18. Especially with chitinase A, the sequence identity is 27.9%, whereas the similarity is as high as 45.5%. As it is shown in Figure 12, the homology of Chi40 with chitinase A is extended to both the TIM barrel and the α + β insertion domains. The N-terminal chitin-binding domain (residues 24–130) of chitinase A, however, has no equivalent in the Chi40 sequence. From the sequence conservation, it turns out that it is quite possible that the structure of Chi40 comprises the analogous structural motifs, that is, the TIM barrel and the α + β insertion.

To our knowledge, these are the first reversible heat denaturation results on a chitinase, and indeed, one of the

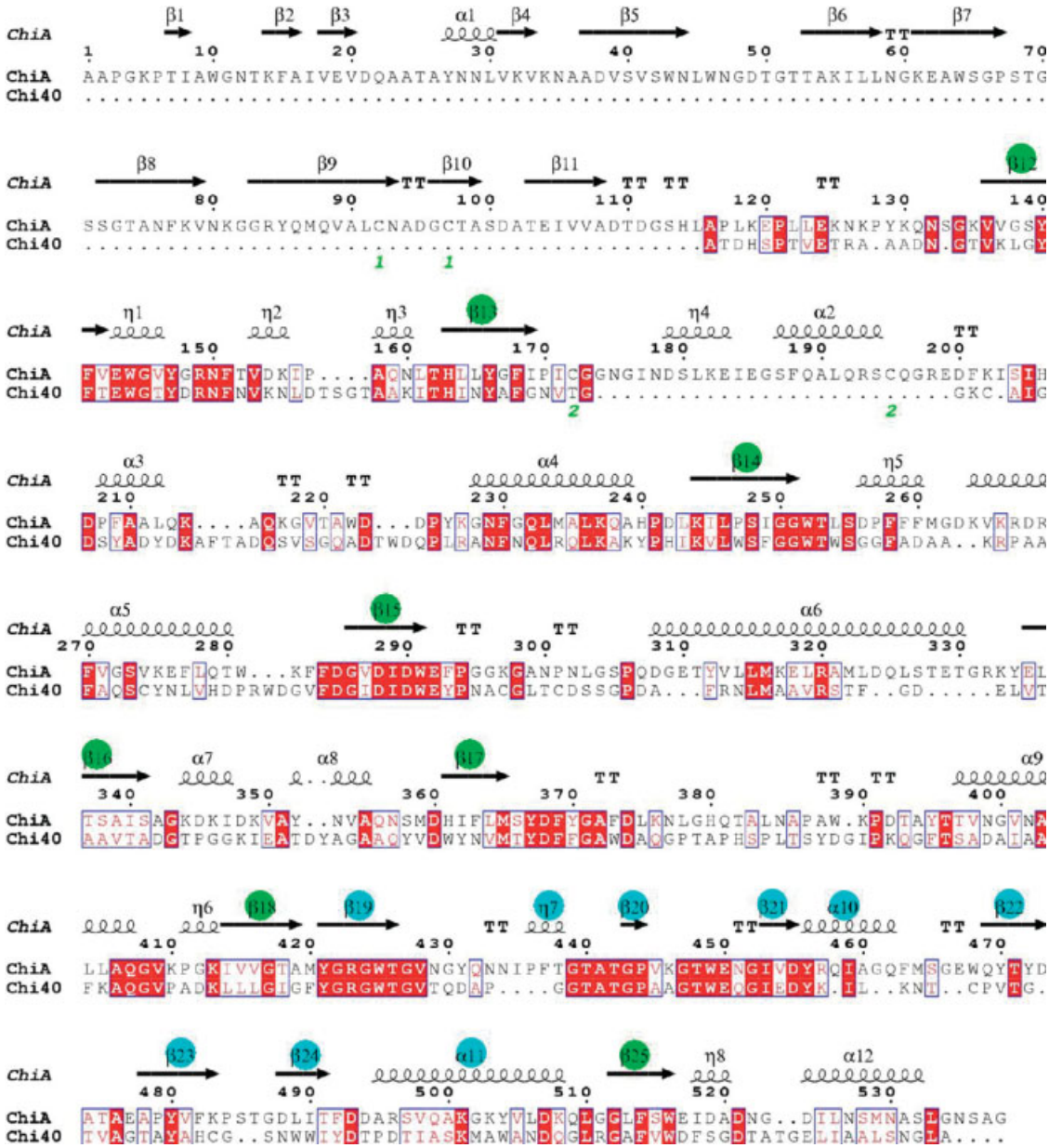

Fig. 12. Sequence alignment of Chi40 and chitinase A (ChiA). Open and red shaded boxes correspond to similarities and identities respectively. Secondary structure elements on the top raw are extracted from the crystal structure of chitinase A (pdb entry: 1CTN[3]). β-Strands colored in green constitute the TIM-barrel domain of chitinase A, whereas secondary structure elements colored in cyan correspond to the α + β insertion domain. Both regions are highly conserved in the sequence of Chi40. The figure was produced with the ESPrint utility.[28]

very few thermal denaturation results on a type-(β/α) barrel protein. Based on the calorimetric results, it has been shown that Chi40 is not a thermodynamically unified domain. The existence of at least one unfolding intermediate fold is required for the thermodynamic description of the thermal transition. This is in accordance to a series of findings concerning the folding mechanism of TIM barrel proteins. Whether the folding intermediate is related solely to the α + β insertion domain is yet to proved.

ACKNOWLEDGMENTS

S.P. acknowledges support from the Graduate Fellowship Program of NCSR "Demokritos." Experimental assistance from M. Papadovasilaki and A. Thanassoulas is acknowledged, as well as the use of the facilities of the Centre for Crystallographic Studies of Macromolecules of NCSR "Demokritos." This work was supported by funding provided by the General Secretariat of Research and Technology of Greece.

REFERENCES

1. Henrissat B, Bairoch A. Updating the sequence-based classification of glycosyl hydrolases. Biochem J 1996;316(Pt 2):695–696.
2. Davies GJ, Tolley SP, Henrissat B, Hjort C, Schulein M. Structures of oligosaccharide-bound forms of the endoglucanase V from *Humicola insolens* at 1.9 A resolution. Biochemistry 1995;34: 16210–16220.

3. Perrakis A, Tews I, Dauter Z, Oppenheim AB, Chet I, Wilson KS, Vorgias CE. Crystal structure of a bacterial chitinase at 2.3 A resolution. Structure 1994;2:1169–1180.
4. Tews I, Vincentelli R, Vorgias CE. N-Acetylglucosaminidase (chitobiase) from *Serratia marcescens*: gene sequence, and protein production and purification in *Escherichia coli*. Gene 1996;170:63–67.
5. Tews I, Perrakis A, Oppenheim A, Dauter Z, Wilson KS, Vorgias CE. Bacterial chitobiase structure provides insight into catalytic mechanism and the basis of Tay-Sachs disease. Nat Struct Biol 1996;3:638–648.
6. Drouillard S, Armand S, Davies GJ, Vorgias CE, Henrissat B. *Serratia marcescens* chitobiase is a retaining glycosidase utilizing substrate acetamido group participation. Biochem J 1997;328(Pt 3):945–949.
7. Prag G, Papanikolau Y, Tavlas G, Vorgias CE, Petratos K, Oppenheim AB. Structures of chitobiase mutants complexed with the substrate Di-N-acetyl-d-glucosamine: the catalytic role of the conserved acidic pair, aspartate 539 and glutamate 540. J Mol Biol 2000;300:611–617.
8. Papanikolau Y, Prag G, Tavlas G, Vorgias CE, Oppenheim AB, Petratos K. High resolution structural analyses of mutant chitinase A complexes with substrates provide new insight into the mechanism of catalysis. Biochemistry 2001;40:11338–11343.
9. Papanikolau Y, Tavlas G, Vorgias CE, Petratos K. De novo purification scheme and crystallization conditions yield high-resolution structures of chitinase A and its complex with the inhibitor allosamidin. Acta Crystallogr D Biol Crystallogr 2003;59:400–403.
10. Christodoulou E, Duffner F, Vorgias CE. Overexpression, purification, and characterization of a thermostable chitinase (Chi40) from *Streptomyces thermoviolaceus* OPC-520. Protein Expr Purif 2001;23:97–105.
11. van Aalten DM, Komander D, Synstad B, Gaseidnes S, Peter MG, Eijsink VG. Structural insights into the catalytic mechanism of a family 18 exo-chitinase. Proc Natl Acad Sci USA 2001;98:8979–8984.
12. Bortone K, Monzingo AF, Ernst S, Robertus JD. The structure of an allosamidin complex with the *Coccidioides immitis* chitinase defines a role for a second acid residue in substrate-assisted mechanism. J Mol Biol 2002;320:293–302.
13. Fusetti F, von Moeller H, Houston D, Rozeboom HJ, Dijkstra BW, Boot RG, Aerts JM, van Aalten DM. Structure of human chitotriosidase. Implications for specific inhibitor design and function of mammalian chitinase-like lectins. J Biol Chem 2002;277:25537–25544.
14. Reardon D, Farber GK. The structure and evolution of alpha/beta barrel proteins. FASEB J 1995;9:497–503.
15. Zitzewitz JA, Gualfetti PJ, Perkons IA, Wasta SA, Matthews CR. Identifying the structural boundaries of independent folding domains in the alpha subunit of tryptophan synthase, a beta/alpha barrel protein. Protein Sci 1999;8:1200–1209.
16. Matthews CR, Crisanti MM. Urea-induced unfolding of the alpha subunit of tryptophan synthase: evidence for a multistate process. Biochemistry 1981;20:784–792.
17. Saab-Rincon G, Froebe CL, Matthews CR. Urea-induced unfolding of the alpha subunit of tryptophan synthase: one-dimensional proton NMR evidence for residual structure near histidine-92 at high denaturant concentration. Biochemistry 1993;32:13981–13990.
18. Gualfetti PJ, Bilsel O, Matthews CR. The progressive development of structure and stability during the equilibrium folding of the alpha subunit of tryptophan synthase from *Escherichia coli*. Protein Sci 1999;8:1623–1635.
19. Godzik A, Skolnick J, Kolinski A. Simulations of the folding pathway of triose phosphate isomerase-type alpha/beta barrel proteins. Proc Natl Acad Sci USA 1992;89:2629–2633.
20. Wintrode PL, Rojsajjakul T, Vadrevu R, Matthews CR, Smith DL. An obligatory intermediate controls the folding of the alpha-subunit of tryptophan synthase, a TIM barrel protein. J Mol Biol 2005;347:911–919.
21. Eder J, Kirschner K. Stable substructures of eightfold beta alpha-barrel proteins: fragment complementation of phosphoribosylanthranilate isomerase. Biochemistry 1992;31:3617–3625.
22. Jasanoff A, Davis B, Fersht AR. Detection of an intermediate in the folding of the (beta alpha)8-barrel N-(5′-phosphoribosyl)anthranilate isomerase from *Escherichia coli*. Biochemistry 1994;33:6350–6355.
23. Pan H, Raza AS, Smith DL. Equilibrium and kinetic folding of rabbit muscle triosephosphate isomerase by hydrogen exchange mass spectrometry. J Mol Biol 2004;336:1251–1263.
24. Plotnikov VV, Brandts JM, Lin LN, Brandts JF. A new ultrasensitive scanning calorimeter. Anal Biochem 1997;250:237–244.
25. Takahashi K, Sturtevant JM. Thermal denaturation of streptomyces subtilisin inhibitor, subtilisin BPN′, and the inhibitor–subtilisin complex. Biochemistry 1981;20:6185–6190.
26. Mayorga OL, Freire E. Dynamic analysis of differential scanning calorimetry data. Biophys Chem 1987;27:87–96.
27. Thompson JD, Higgins DG, Gibson TJ. CLUSTAL W: improving the sensitivity of progressive multiple sequence alignment through sequence weighting, position-specific gap penalties and weight matrix choice. Nucleic Acids Res 1994;22:4673–4680.
28. Gouet P, Courcelle E, Stuart DI, Metoz F. ESPript: analysis of multiple sequence alignments in PostScript. Bioinformatics 1999;15:305–308.
29. Freire E, van Osdol WW, Mayorga OL, Sanchez-Ruiz JM. Calorimetrically determined dynamics of complex unfolding transitions in proteins. Annu Rev Biophys Biophys Chem 1990;19:159–188.
30. Sanchez-Ruiz JM. Differential scanning calorimetry of proteins. In: Biswas BB, Siddhartha R, editors. Proteins: Structure, Function, and Engineering (Subcellular Biochemistry). New York: Plenum Press; 1995. p. 133–176.
31. Plaza del Pino IM, Pace CN, Freire E. Temperature and guanidine hydrochloride dependence of the structural stability of ribonuclease T1. Biochemistry 1992;31:11196–11202.
32. Sturtevant JM. Biochemical apllications of differential scanning calorimetry. Annu Rev Phys Chem 1987;38:463–488.
33. Freire E, Biltonen RL. Thermodynamics of transfer ribonucleic acids: the effect of sodium on the thermal unfolding of yeast tRNAPhe. Biopolymers 1978;17:1257–1272.
34. Privalov PL, Mateo PL, Khechinashvili NN, Stepanov VM, Revina LP. Comparative thermodynamic study of pepsinogen and pepsin structure. J Mol Biol 1981;152:445–464.
35. Kidokoro S, Wada A. Determination of thermodynamic functions from scanning calorimetry data. Biopolymers 1987;26:213–229.
36. Privalov PL, Potekhin SA. Scanning microcalorimetry in studying temperature-induced changes in proteins. Methods Enzymol 1986;131:4–51.
37. Griko YV, Freire E, Privalov G, van Dael H, Privalov PL. The unfolding thermodynamics of c-type lysozymes: a calorimetric study of the heat denaturation of equine lysozyme. J Mol Biol 1995;252:447–459.
38. Honda S, Uedaira H, Vonderviszt F, Kidokoro S, Namba K. Folding energetics of a multidomain protein, flagellin. J Mol Biol 1999;293:719–732.
39. Murphy KP, Freire E. Thermodynamics of structural stability and cooperative folding behavior in proteins. Adv Protein Chem 1992;43:313–361.
40. Tanaka A, Kobayashi D, Senoo K, Obata H. Possibility for discriminating between two representative non two-state thermal unfolding models of proteins by DSC. Biosci Biotechnol Biochem 1999;63:438–442.
41. Vogl T, Jatzke C, Hinz HJ, Benz J, Huber R. Thermodynamic stability of annexin V E17G: equilibrium parameters from an irreversible unfolding reaction. Biochemistry 1997;36:1657–1668.
42. Benitez-Cardoza CG, Rojo-Dominguez A, Hernandez-Arana A. Temperature-induced denaturation and renaturation of triosephosphate isomerase from *Saccharomyces cerevisiae*: evidence of dimerization coupled to refolding of the thermally unfolded protein. Biochemistry 2001;40:9049–9058.
43. Privalov PL. Stability of proteins: small globular proteins. Adv Protein Chem 1979;33:167–241.
44. Becktel WJ, Schellman JA. Protein stability curves. Biopolymers 1987;26:1859–1877.
45. Andrade MA, Chacon P, Merelo JJ, Moran F. Evaluation of secondary structure of proteins from UV circular dichroism spectra using an unsupervised learning neural network. Protein Eng 1993;6:383–390.
46. Kabsch W, Sander C. Dictionary of protein secondary structure: pattern recognition of hydrogen-bonded and geometrical features. Biopolymers 1983;22:2577–2637.
47. Provencher SW, Glockner J. Estimation of globular protein second-

ary structure from circular dichroism. Biochemistry 1981;20:33–37.
48. Sreerama N, Woody RW. Protein secondary structure from circular dichroism spectroscopy. Combining variable selection principle and cluster analysis with neural network, ridge regression and self-consistent methods. J Mol Biol 1994;242:497–507.
49. Bohm G, Muhr R, Jaenicke R. Quantitative analysis of protein far UV circular dichroism spectra by neural networks. Protein Eng 1992;5:191–195.
50. Sanchez-Ruiz JM, Lopez-Lacomba JL, Cortijo M, Mateo PL. Differential scanning calorimetry of the irreversible thermal denaturation of thermolysin. Biochemistry 1988;27:1648–1652.
51. Sanchez-Ruiz JM. Theoretical-analysis of Lumry-Eyring models in differential scanning calorimetry. Biophys J 1992;61:921–935.
52. Ramsay G, Montgomery D, Berger D, Freire E. Energetics of diphtheria toxin membrane insertion and translocation: calorimetric characterization of the acid pH induced transition. Biochemistry 1989;28:529–533.
53. Davoodi J, Wakarchuk WW, Surewicz WK, Carey PR. Scan-rate dependence in protein calorimetry: the reversible transitions of *Bacillus circulans* xylanase and a disulfide-bridge mutant. Protein Sci 1998;7:1538–1544.
54. Dragan AI, Potekhin SA, Sivolob A, Lu M, Privalov PL. Kinetics and thermodynamics of the unfolding and refolding of the three-stranded alpha-helical coiled coil, Lpp-56. Biochemistry 2004;43:14891–14900.
55. Schmid XF. Kinetics of unfolding and refolding of single-domain proteins. In: Creighton ET, editor. Protein Folding. New York: W.H. Freeman and Co.; 1992. p. 197–241.
56. Stewart DE, Sarkar A, Wampler JE. Occurrence and role of *cis* peptide bonds in protein structures. J Mol Biol 1990;214:253–260.
57. Creighton ET. Possible implications of many proline residues for the kinetics of protein unfolding and refolding. J Mol Biol 1978;125:401–406.
58. Garel J-R. Folding of large proteins: multidomain and multisubunit proteins. In: Creighton ET, editor. Protein folding. New York: W.H. Freeman and Co.; 1992. p 405–454.
59. Wu Y, Matthews CR. A *cis*-prolyl peptide bond isomerization dominates the folding of the alpha subunit of Trp synthase, a TIM barrel protein. J Mol Biol 2002;322:7–13.
60. Odefey C, Mayr LM, Schmid FX. Non-prolyl *cis-trans* peptide bond isomerization as a rate-determining step in protein unfolding and refolding. J Mol Biol 1995;245:69–78.
61. Matsumoto T, Nonaka T, Hashimoto M, Watanabe T, Mitsui Y. Three-dimensional structure of the catalytic domain of chitinase A1 from *Bacillus circulans* Wl-12 at a very high resolution. Proc Jpn Acad Ser B 1999;75:269–274.